EBSD CHARACTERIZATION OF HAZ FROM SINGLE AND MULTI-PASS WELDING OF NIOBIUM MICROALLOYED LINEPIPE STEELS

Sundaresa Subramanian [1], Yang You[2], Wenjin Nie [2, 3], Chengliang Miao [2], Chengjia Shang [2], Xiaobing Zhang[3] and Laurie Collins [4]

[1] Department of Mat. Sci. and Eng., McMaster University, Hamilton, Canada
[2] School of Mat. Sci. and Eng, University of Sci. and Tech., Beijing, China
[3] Sha-Steel Company, China
[4] Evraz Inc. NA, Regina, SK, Canada

Keywords: Linepipe Steels, HAZ Toughness, Welding, EBSD, CGHAZ, IRCGHAZ, High Angle Boundaries, Microalloying, Niobium

Abstract

EBSD studies on the HAZ have confirmed that there is significant loss in the density (number count per unit area) of high angle boundaries in HAZ regions in single-pass welding from high heat inputs (>35 kJ/cm). The microstructure is deprived of microcrack arresters due to loss of high angle boundaries at slow cooling rates (high t8/5), when transformation is controlled by a thermally activated diffusion mechanism. Thus, in the absence of crack arresters, any microcrack nucleated by hard and brittle MA product could grow to attain the Griffith critical crack length to initiate brittle fracture in accordance with the Cottrell-Petch model. The research has identified the target microstructure with optimum density and dispersion of crystallographic high angle boundaries required to obtain maximum toughness at low temperature in the HAZ region in single-pass welding associated with a low temperature window of transformation in higher niobium bearing higher grade linepipe steels.

The effect of increasing heat input of welding on the hierarchical evolution of microstructure and crystallographic high angle boundaries within austenite grains in the HAZ was investigated in higher Nb microalloyed higher grade (X80 and X100) linepipe steels. Pole figure analysis of crystallographic data captured by EBSD analysis is used to identify crystallographic relationships of coherent transformation products with the parent austenite grains. It is shown that high angle boundaries are formed between crystallographic units with different Bain groups within each packet upon coherent transformation of austenite grain in the target microstructure with maximum toughness. This work has demonstrated that a uniform dispersion of high density of high angle boundaries, due to large misorientations between different Bain groups occurring within austenite grains, could be promoted by a low temperature window of transformation associated with an optimum cooling rate.

Niobium addition is effective in lowering the transformation temperature because niobium dissolved in the matrix inhibits ferrite nucleation at austenite grain boundaries. Further, interphase precipitation of NbC retards growth of ferrite grains. Thus niobium addition is beneficial in lowering the transformation temperature to obtain a high density of high angle boundaries due to large misorientations between different Bain groups occurring within austenite grains in single-pass welding.

In multi-pass low heat input welds typical of the pipeline girth welding process, the effect of nickel addition on structure and toughness of inter-critically reheated coarse grained austenite, IRCGHAZ was investigated with simulated weld thermal cycles. High Ni addition to Nb microalloyed steel is shown to increase the toughness compared with low Ni in both CGHAZ and IRCGHAZ. This is attributed to suppression of both MA formed from continuous cooling in the CGHAZ and massive MA along prior austenite grain boundaries in the IRCGHAZ.

Introduction

Over the past decade, there has been considerable effort directed to the development of line pipe suitable for Arctic applications. In North America this attention has focused on the requirements for proposed pipelines to transport natural gas from the Mackenzie delta in Canada (the Mackenzie Gas project) or from northern Alaska to the existing pipeline networks in Alberta. In view of the long distances involved, efficient gas transport demands high operating pressures, which translate into requirements for both high strength steel (yield strength 80 to 100 ksi or 560 to 700 MPa) and heavy wall thicknesses (up to 25.4 mm). In addition, consideration of frost heave or settling where the pipeline passes through regions of continuous or discontinuous permafrost has resulted in the application of strain-based designs which allow for application of significant tensile strains in the longitudinal direction. While the base material exhibits good ductility and toughness, concern exists regarding the ability of circumferential welds and the associated heat affected zones to withstand such strains and provide the requisite fracture toughness.

In addition to the stringent property requirements that will be imposed on circumferential welds by strain-based designs, the pipeline industry is also moving to adopt more efficient welding practices. Dual torch, Tandem welding and Dual Tandem welding practices have been explored. While such practices are effective in increasing welding speeds, they expose the material in the heat affected zone to thermal cycles which may be considerably different from those associated with conventional single torch gas metal arc welds (GMAW). In view of the increasingly stringent properties requirements arising from strain-based designs and the unconventional thermal cycles imposed by new welding techniques, it is important to understand the evolution of microstructure in the weld HAZ and the relationship between that microstructure and the final material properties.

A series of projects have been undertaken to investigate the relationship between the welding thermal cycle, microstructure development and the resultant mechanical properties. Ideally the goal is to develop a steel chemistry that develops a strong, tough microstructure when subjected to a wide range of welding conditions. Initial work by Volkers, Collins and Hamad [1] demonstrated a correlation between reduced HAZ toughness and a coarser prior austenite grain size developed during dual torch welding. Further work with the University of British Columbia has sought first to characterize the thermal cycle associated with dual torch welding and secondly to understand austenite grain coarsening, and Nb dissolution and re-precipitation behavior in Nb microalloyed steels as a result of different thermal cycles [2]. In addition to prior austenite grain size, the transformed microstructure which results after heating and subsequent cooling will also influence fracture toughness. The work of Penniston et al. confirmed that the elimination of coarse TiN particles by control of Ti and N content of the steel resulted in enhanced toughness [3]. Investigation of steels with variations in carbon content by Penniston et al. also suggested

that steels with finer lath structures were more resistant to crack propagation [4]. It is the evolution of microstructural morphology, and crystallographic misorientations super-posed on the microstructure in HAZ region of Nb microalloyed steel, which is the subject of the present study. In particular, this paper is based on EBSD characterization of the HAZ region. Phenomenological studies are carried out on (i) MA product in l microstructure, (ii) hierarchical evolution of crystallographic structure of transformation product from parent austenite grains, and (iii) density and dispersion of crystallographic high angle boundaries of the lath structure in the HAZ region. The work is aimed at optimizing target microstucture to improve fracture toughness of the HAZ region arising from single and multi-pass welding of Nb microalloyed steels by minimizing MA product, and retaining an adequate density of high angle boundaries to arrest micro-cracks.

Experimental Methodology

The effect of increasing heat input on HAZ microstructure and HAZ toughness was investigated in X80 grade higher niobium steel designed for high temperature processing (HTP) and higher niobium X100 multi-phase steel using Gleeble simulation of single pass welding. The effect of nickel addition on CGHAZ and IRCGHAZ microstructure and HAZ toughness of Nb bearing plates was investigated using Gleeble simulation of low heat input welding. Optical, SEM and EBSD techniques were used for microstructural characterization.

EBSD data were analyzed to determine the density and dispersion of high angle boundaries of the crystallographic structure super-posed on the microstructural morphology. Pole figure analysis was used to determine the crystallographic orientation relationship of transformation product to parent austenite grains, and to elucidate the hierarchical evolution of high angle boundaries associated with misorientations arising from intersection of regions with different Bain groups [5]. The distribution of residual austenite associated with MA product was mapped. Charpy tests at -20 ºC were carried out on test specimens from Gleeble simulation of HAZ regions for different heat inputs. Brittle fracture behavior was correlated with density and dispersion of high angle boundaries as well as morphology and dispersion of MA product. EBSD results were used to identify and benchmark target microstructure with crystallographic high angle boundaries.

Results

1. Studies on HAZ from Single Pass Welding of X-80 Grade Higher Nb Low Interstitial (HTP) Steel

The effect of heat input on CGHAZ of single-pass welding of HTP steel was investigated. Table I summarizes the base chemistry of the steel. Table II summarizes the time to cool between 800 to 500 ºC, t8/5, for different heat input and corresponding cooling rates for welding 25.2 mm thickness plate. Figure 1 shows the average Charpy impact energies at -20 ºC for different heat inputs in Gleeble weld simulation samples. A heating rate of 130 ºC/s and a peak temperature of 1300 ºC were used.

Table I. Base Chemistry of the Steel (wt.%)

C	Mn	Si	Nb	Al+Ti+Cu+Cr
0.04	1.75	0.22	0.10	0.53

Table II. Heat Inputs, Corresponding t8/5 and Cooling Rate (Plate Thickness: 25.2 mm)

Heat input kJ/cm	t8/5 s	Cooling rate during 800~500 ºC ºC/s
16	5.7	52.6
20	9.5	31.6
30	21.6	13.9
40	39.3	7.6
50	58.7	5.1
58	80.9	3.7

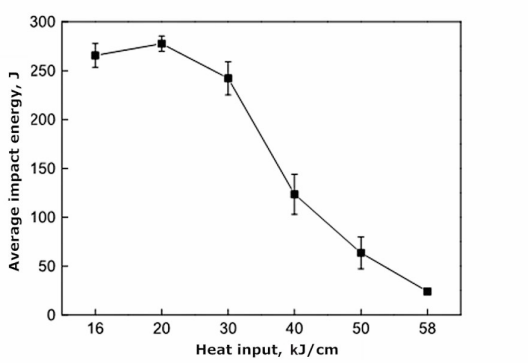

Figure 1. Charpy impact energy at -20 ºC for different heat inputs.

The best toughness is obtained for a heat input of 20 kJ/cm which corresponds to a cooling rate of 30 ºC/s, Figure 1. Figure 2 shows the distribution of austenite grains for different heat inputs. Note that a high fraction of coarse austenite grain size is obtained with a high heat input of 40 kJ/cm and above. It is noteworthy that varying cooling rates between 3 to 30 ºC/s had only a marginal effect on average prior austenite grain size, but a very substantial reduction in impact energy is observed as cooling rate is reduced. However, the brittle fracture initiation should be related to the coarsest austenite grains and not the average grain size. Figure 3 shows the variation of MA and matrix microstructure with increasing heat input from 20, 30, 50 and 58 kJ/cm. At low heat input, fine MA product is dispersed in the lath structure corresponding to t8/5 of 10-20 s. At high heat input, corresponding to t8/5 of 60 to 90 s, coarse particles occur which are considered to be MA product associated with granular bainite.

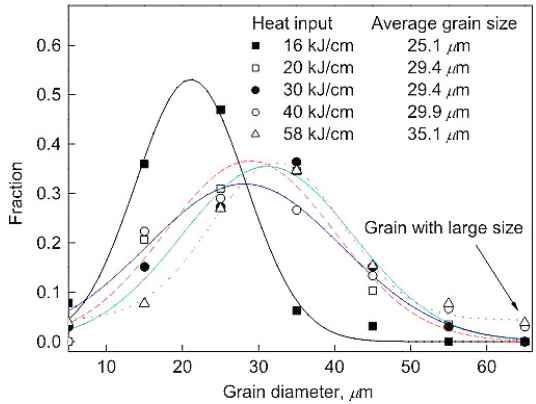

Figure 2. Distributions of prior austenite grain size for different heat inputs.

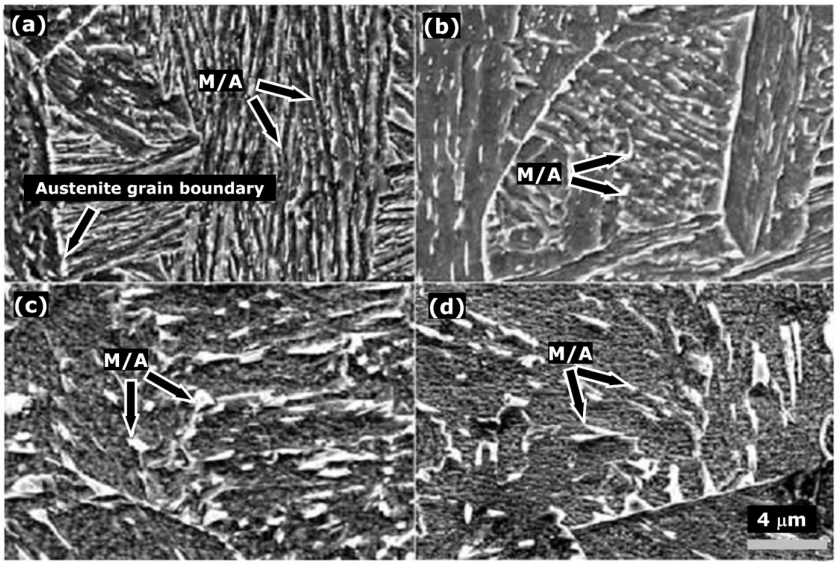

Figure 3. SEM images of microstructures of the samples under heat inputs of 20 kJ/cm (a), 30 kJ/cm (b), 50 kJ/cm (c) and 58 kJ/cm (d), showing fine MA constituents dispersed in a lath structure under low heat inputs, becoming coarse MA particles in granular bainite under high heat inputs.

Figure 4 shows high angle boundaries with crystallographic boundary misorientation > 45 degrees mapped on the microstructure. High density and dispersion of high angle boundaries is retained at heat input of 20 kJ/cm corresponding to a high cooling rate of 30 ºC/s. However, the density and dispersion of high angle boundaries are significantly decreased at the higher heat input of 50 kJ/cm. Since the high angle boundaries above 45 degrees are shown to be effective in deflecting cracks, these are potential micro-crack arresters [6]. In their absence, micro-crack could grow to reach the critical Griffith crack length to initiate brittle fracture.

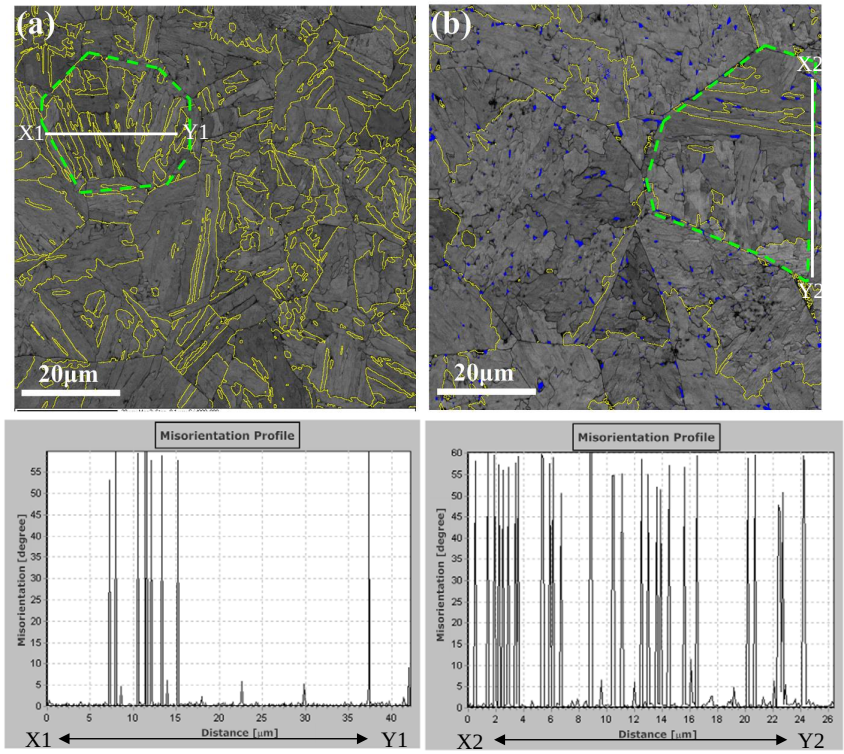

Figure 4. Band contrast maps with high angle boundaries dispersion above 45° for samples under heat input of 20 kJ/cm(a), and 50 kJ/cm(b) (Grey areas: ferrite (bcc); Yellow lines: boundaries above 45°; Blue areas: residual austenite (fcc)). Areas encircled by green dotted line show the prior austenite grains in the two samples. The degree of grain misorientation (high angle boundary) with distance is plotted along the line-scan between X1-Y1 in the Gleeble simulation sample with a low heat input of 20 kJ/cm (a), and X2-Y2 in a sample with high heat input of 50 kJ/cm (b) respectively.

The large spacing between high angle boundaries can be clearly seen in the sample with a high heat input welding of 50 kJ/cm.

The salient observations are that by increasing the heat input from 20 to 50 kJ/cm, (i) a small number of very coarse austenite grains are formed though the average austenite grain size changes only slightly, (ii) the microstructural morphology changes from lath bainite with a fine dispersion of MA product to granular bainite with coarse MA product, (iii) the density and dispersion of high angle boundaries are significantly decreased, and (iv) the Charpy toughness is significantly reduced. At high heat input, coarse MA products act as potential sites for crack initiation. In the absence of high angle boundaries, which could arrest micro-cracks, microcracks could readily grow to attain the Griffith crack length to initiate brittle fracture. The studies on HAZ confirm that there is an optimum welding heat input for a given thickness of plate of HTP chemistry at which toughness properties of HAZ regions are maximized under conditions in which (i) the amount of MA product is low, and it is fine in size and well dispersed in the matrix, and (ii) density of high angle boundaries is high and its dispersion is uniform and (iii) low temperature transformation product with fine lath structure is ensured.

2. Studies of the HAZ from Single Pass Welding of X100 High Nb Multi-Phase Steel

The base chemistry of higher Nb multi-phase X100 steel is given in Table III. Figure 5 shows the optical microstructure of X100 multi-phase steel plate. The ferrite grains are seen at prior austenite grain boundaries with bainitic ferrite in the interior of austenite grains. Table IV shows the mechanical properties of X100 plate. Table V shows the impact toughness and DWTT results at different test temperatures for base plate. Table VI shows heat input, t8/5 for different heat input, and the corresponding cooling rate from 800/500 ^{o}C in welding 14.7 mm thickness plate.

Table III. Chemistry of X100 Multi-Phase Steel (wt.%)

C	Si	Mn	Nb	Ti	Cr	Ni	Mo	Al	N
0.07	0.25	1.94	0.081	0.014	0.28	0.18	0.26	0.035	0.004

Table IV. Mechanical Properties of X100 Multi-Phase Steel

Yield Strength (Rt0.5) MPa	Tensile Strength MPa	Uniform Elongation %	Total Elongation %	Yield/Tensile
708	909	8.0	30	0.78

Table V. Charpy Toughness and DWTT of Base Plate

Testing Temperature ^{o}C	Charpy Impact Energy J	DWTT %
0	255	100
-20	238	100
-40	258	100
-60	224	71
-80	225	56

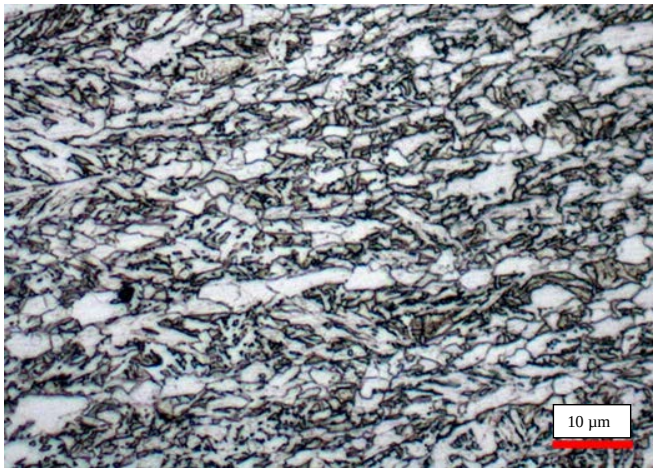

Figure 5. Optical microstructure of X-100 multi-phase steel.

Table VI. Heat Inputs, Corresponding t8/5 and Cooling Rate (Plate Thickness: 14.7 mm)

Heat input kJ/cm	t8/5 s	Cooling rate during 800~500 ºC ºC/s
8	4.8	62.4
16	12.56	23.9
20	19.6	15.3
25	30.6	9.8
30	44.1	6.8
50	122.6	2.4

Figure 6(a) shows the effect of heat input on Charpy toughness from single-pass welding simulation and 6(b) shows the austenite grain size distribution for different heat inputs. The toughness value reaches a maximum at a heat input of 20 kJ/cm. Figure 7 shows optical micrographs of MA product as revealed by special etchants of four samples with heat input of 8, 20, 25 and 50 kJ/cm. The sample with higher heat input of 50 kJ/cm exhibits the coarsest MA product.

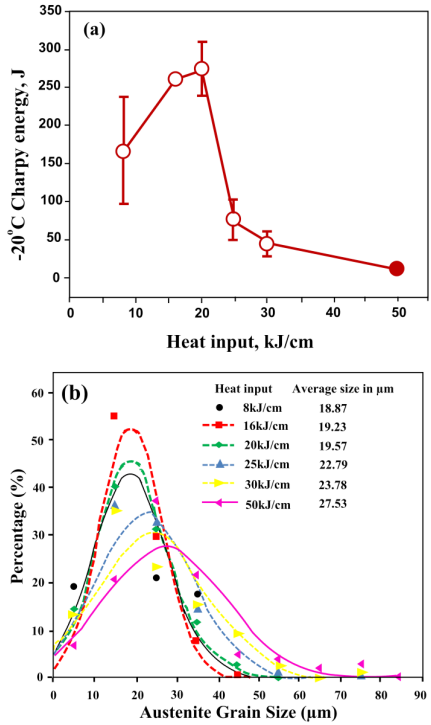

Figure 6. (a) Charpy impact energy of X100 at -20 °C for different heat inputs; (b) Austenite grain size distribution for different heat inputs.

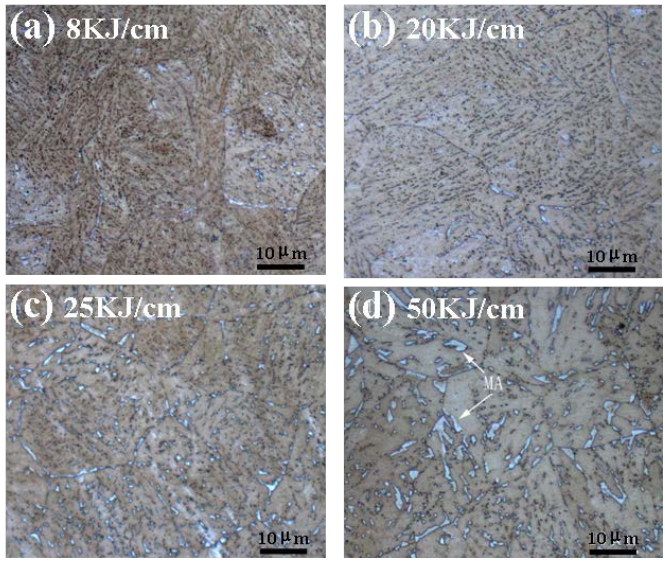

Figure 7. (a), (b), (c) and (d) are optical pictures of MA product revealed in color by special etchant for heat inputs of 8, 20, 25 and 50 kJ/cm respectively in multi-phase X100. Coarse MA products are seen with increasing heat input.

Figure 8 shows a higher density of high angle boundaries in the sample with good toughness obtained with optimum heat input of 20 kJ/cm compared with the low density of high angle boundaries in the sample with low toughness obtained at high heat input (50 kJ/cm) welding. Figure 9 shows pole figure analysis of samples of heat input of 8, 20, 25 and 50 kJ/cm respectively, showing the number of packets[7, 8] within the austenite grain examined. There is no significant change in the number of packets within austenite grains with increasing heat input.

Figure 10 shows the distribution of Bain groups within a packet in each case. Note the uniform distribution of high angle boundaries within a packet in the sample with a low heat input of 20 kJ/cm. Different Bain groups are distinguished by different colors. High angle boundaries arise within a packet when different Bain groups meet, i.e., at the intersection of regions with different colors. *Thus at low heat input, high densities of high angle boundaries arise from misorientations from different Bain groups, whereas very low densities of high angle boundaries are observed at high heat input. More in-depth analysis has confirmed that high density of high angle boundaries is related to low temperature of transformation products associated with high cooling rate, and the microstructural morphology accompanying them.*

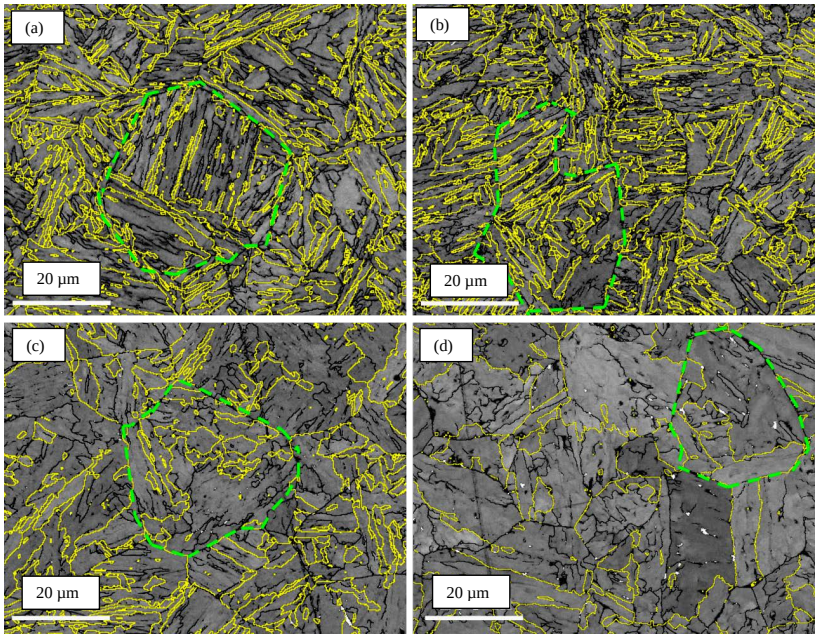

Figure 8. Dispersion of high angle boundaries in the samples with heat input of 8 kJ/cm (a), 20 kJ/cm (b), 25 kJ/cm (c) and 50 kJ/cm (d), (yellow lines - boundaries greater than 45°, green lines - signify prior austenite grain boundary).

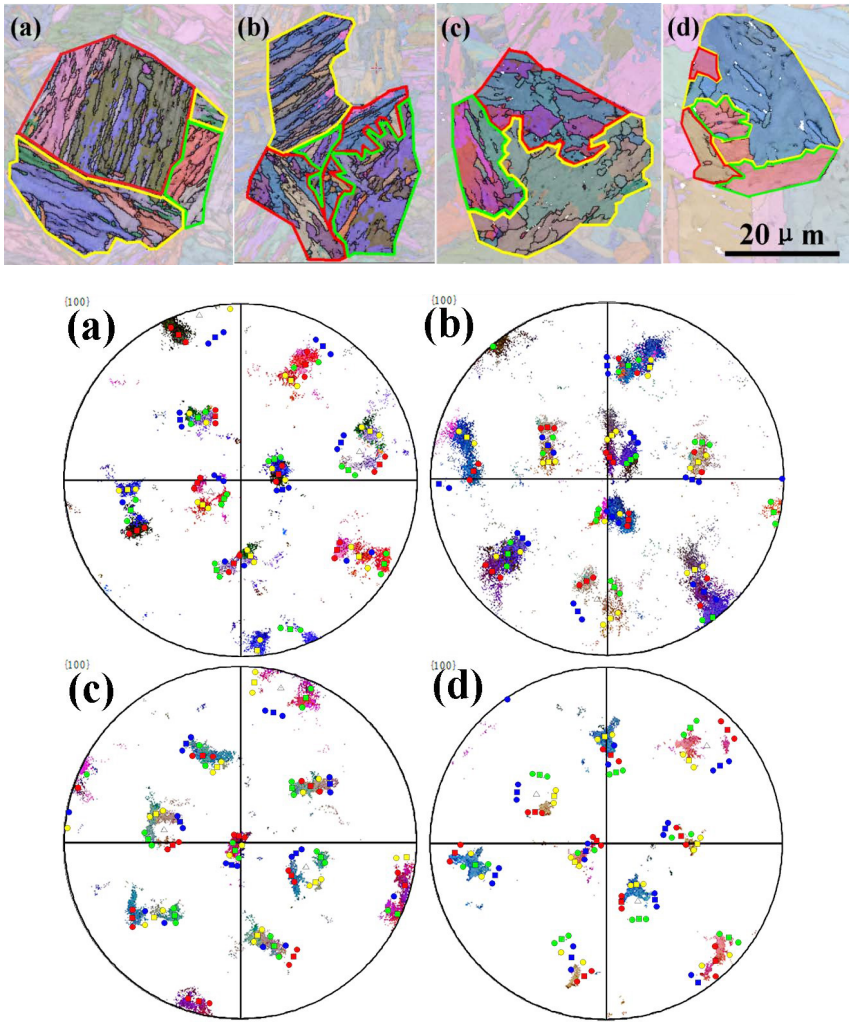

Figure 9. Pole figure analysis of samples of heat input of 8 kJ/cm (a), 20 kJ/cm (b), 25 kJ/cm (c) and 50 kJ/cm (d) respectively, showing the number of packets within the austenite grain examined.

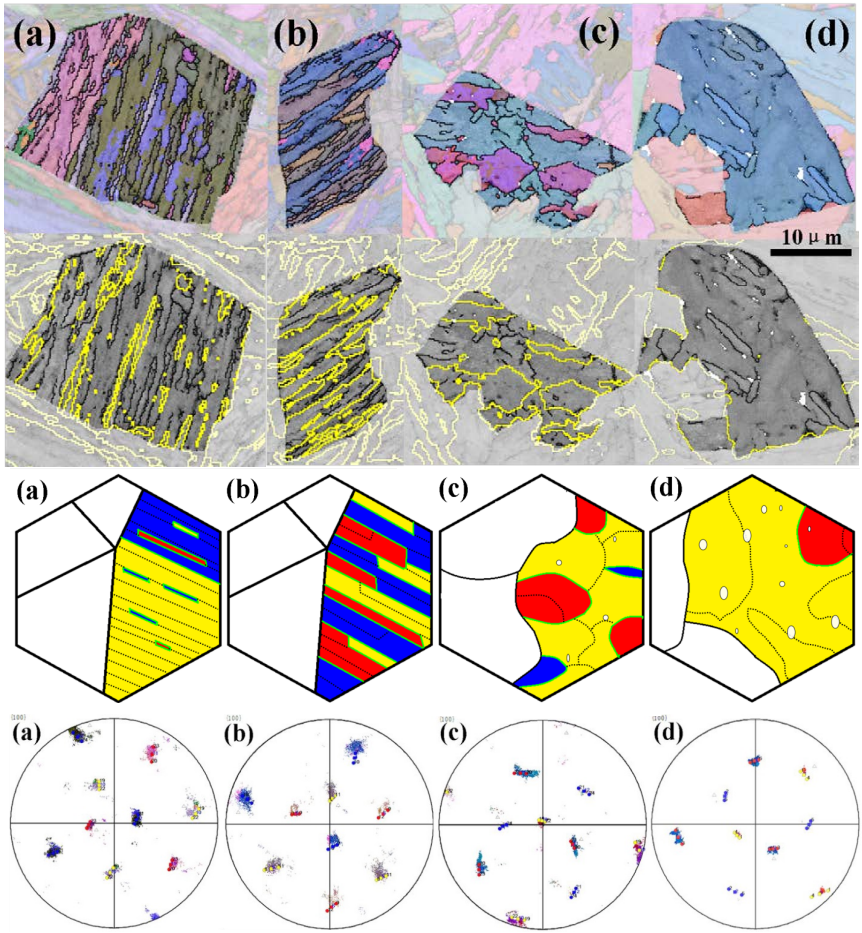

Figure 10. EBSD mapping of regions from 8 kJ/cm (a), 20 kJ/cm (b), 25 kJ/cm (c) and 50 kJ/cm (d). Pole figure analysis is used to distinguish different Bain groups, using different colors to distinguish the different Bain groups. High angle boundaries are formed when crystallographic units with different Bain groups meet, as shown by the schematic diagram. The best distribution of high angle boundaries, from a low heat input of 20 kJ/cm, is found to correlate with the best toughness at -20 ºC.

3. Studies on Alloying Effect of Ni on HAZ Toughness in Multi-Pass Low Heat Input Welding of Nb Microalloyed Plates

Gleeble simulations were carried out to study the effect of increasing Ni addition on toughness of coarse grained austenite in the coarse grain heat affected zone (CGHAZ) from the first pass and the inter-critically reheated coarse grained heat affected zone (IRCGHAZ) from the second pass respectively in low heat input welding (6 kJ/cm) with 12 mm thickness. The base chemistries of the two steels used in the investigation are summarized in Table VII. The toughness values from the base metal, single pass and sub-zones corresponding to different reheat temperatures in the second pass are summarized in Table VIII. The Charpy toughness is plotted for each case with specific metallurgical history for the first and second passes in Figure 11.

Table VII. Chemistry of the Low Ni and Higher Ni Steels (wt %)

Sample	C	Si	Mn	Nb	Ti	Cr	Mo	Cu	Ni
Low Ni	0.050	0.26	1.43	0.054	0.022	0.26	0.32	0.72	0.81
High Ni	0.049	0.26	1.44	0.052	0.013	0.27	0.33	0.78	3.74

Table VIII. Charpy Toughness of Base Plate, First Pass HAZ and Second Pass Sub-Zones

	Sample	Base plate	HAZ in pass I	Sub-zones in HAZ after pass II simulation at different Temp., ºC					
				1000	900	850	800	750	700
-20 ºC Charpy energy in J	Low Ni	51.8	61	54	49	47	36	54	61
	High Ni	120.5	92	106	91	84	78	66	84

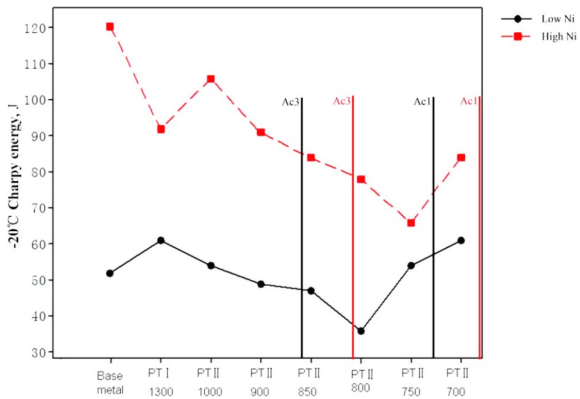

Figure 11. Charpy toughness of base plate, first pass HAZ and second pass sub-zones (Low Ni: Ac1=726 ºC, Ac3=863 ºC; High Ni: Ac1=678 ºC, Ac3=813 ºC. Passes I and II and associated temperatures).

SEM pictures of high and low Ni samples from single pass welding with a low heat input (6 kJ/cm) are shown in Figure 12. These show an apparently comparable distribution of MA product, though the high nickel addition gives an increased Charpy toughness. Figure 13 shows pole figure analysis of selected austenite grains from the CGHAZs of low and high nickel samples in single-pass welding. Based on the crystallographic relationship between a parent austenite grain and its coherent transformation products [5], the real orientation of austenite is distinguished from mis-indexed ones by pole figure analysis. The real orientation data of austenite from the corresponding position on the pole figure for the low Ni sample indicate a greater amount of residual austenite than the high nickel sample. Figure 14 shows islands of residual austenite occur beside bcc structures, and the bcc structure here is indicative of the presence of martensite. High angle boundaries associated with islands of MA are not desirable as high carbon MA will aid brittle fracture. Hence high angle boundaries associated with MA product are not desirable.

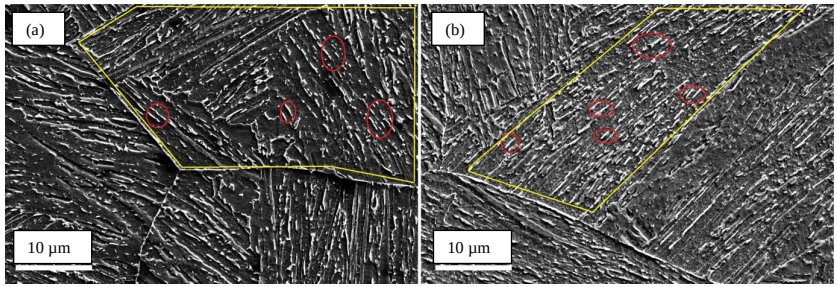

Figure 12. SEM pictures of low (a) and high Ni (b) from single pass welding at low heat input, showing comparable dispersion of MA product.

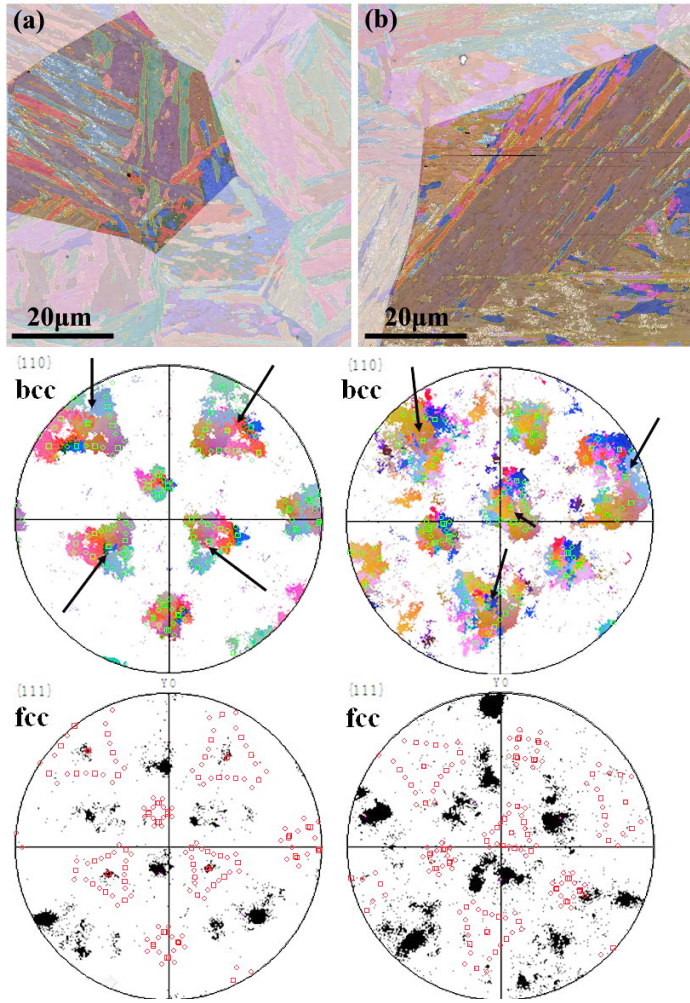

Figure 13. Pole figure analysis of a selected austenite grain from low (a) and high Ni (b) samples from CGHAZ from single pass welding. Low Ni sample exhibits clearly higher amount of residual austenite than high Ni sample.

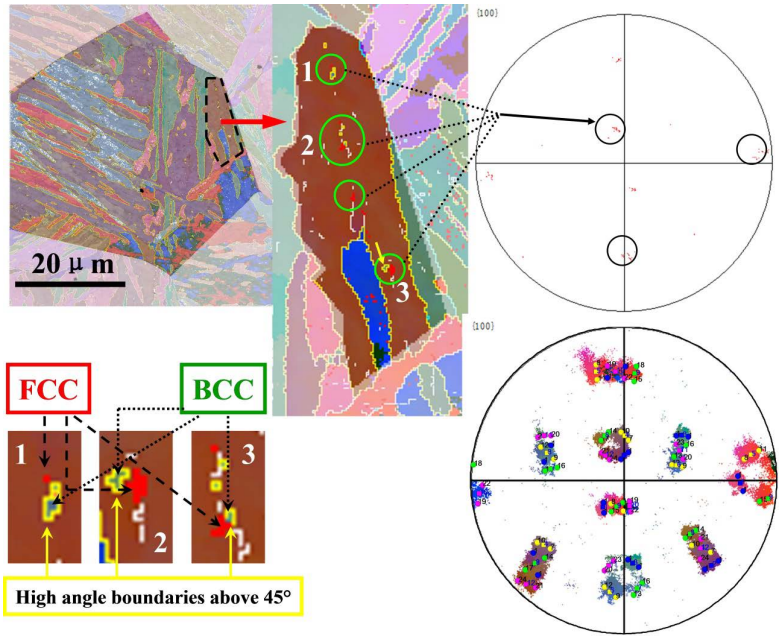

Figure 14. Islands of residual austenite are clearly identified in low Ni alloy using pole figure analysis in the region, which are probably associated with high carbon MA. High angle boundaries associated with such MA product are not desirable, as they will initiate brittle fracture.

From Gleeble simulation of multi-pass welding of the low and high Ni samples: Figure 15 shows optical and SEM pictures of the simulated IRCGHAZ of low Ni (800 ºC) and high Ni (750 ºC), corresponding to the lowest toughness in each case. The dark arrows point to massive MA occurring at prior austenite grain boundaries, forming a necklace around each grain in the low Ni sample. By increasing the nickel content, massive MA is suppressed. There is aligned MA present within each grain in both low and high Ni samples.

Figure 16 is the Euler diagram for the low Ni sample, exhibiting massive MA at austenite boundaries and aligned MA within the austenite grain. There is a close correspondence of these results with the SEM picture of Li and Baker [9], which is shown alongside.

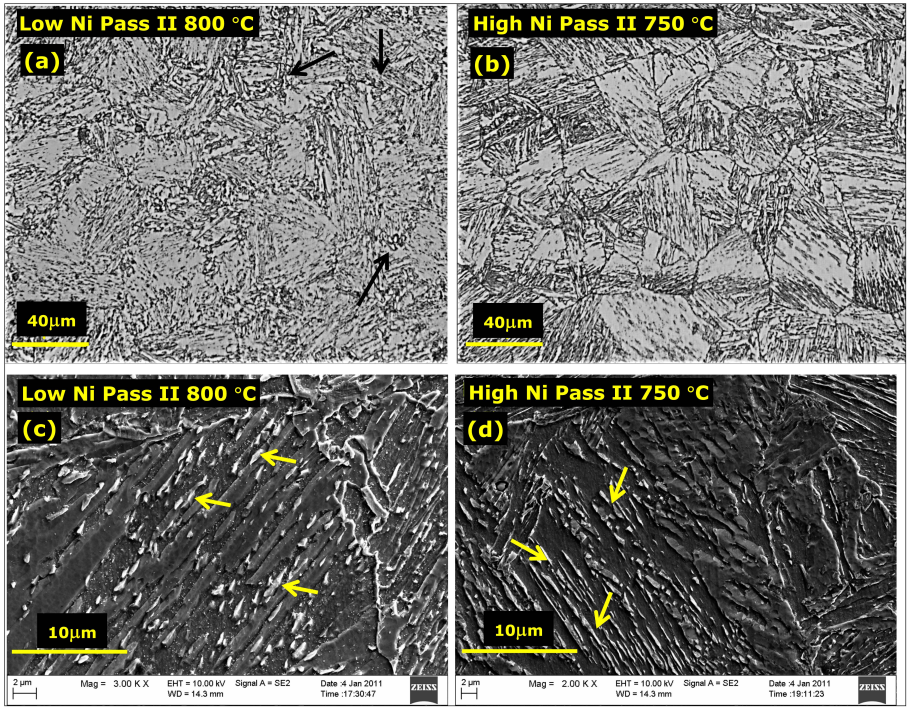

Figure 15. Optical micrographs and SEM pictures of the Gleeble simulated IRCGHAZ of low Ni (800 ºC) and high Ni (750 ºC) respectively, corresponding to the lowest toughness in each case. The dark arrows point to massive MA forming a necklace around prior austenite grain boundaries in the low Ni sample. By increasing the nickel content, massive MA is suppressed. There is aligned MA occurring within each grain in both low and high Ni samples, as indicated by yellow arrows.

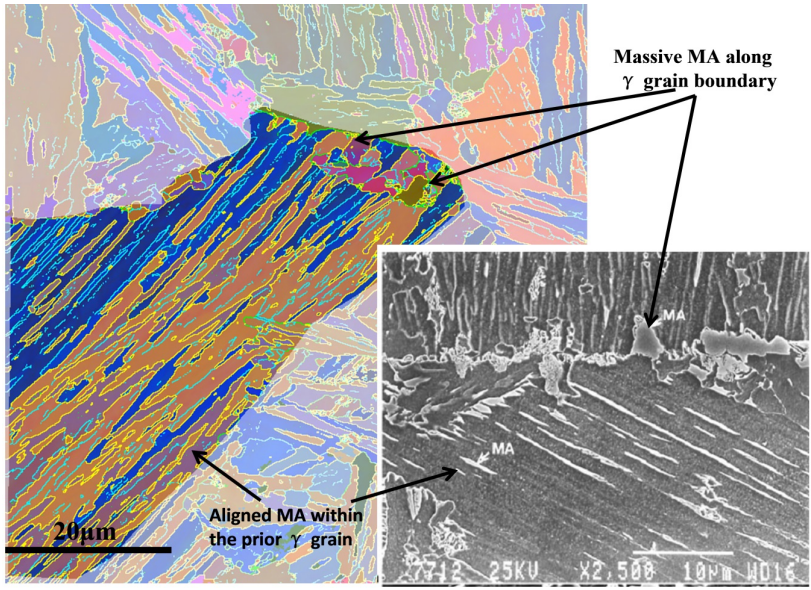

Figure 16. Euler diagram of low Ni sample exhibiting massive MA at austenite boundaries and aligned MA within the austenite grain. There is a close correspondence of these results with the SEM picture of Li and Baker [9], which is shown alongside.

Figure 17 shows band contrast maps of low Ni (a) and high Ni (b) respectively. The dark areas found in the massive MA in low Ni are confirmed by pole figure analysis to exhibit Kurdjumov-Sachs (K-S) variants, characteristic of martensite as shown in Figure 18.

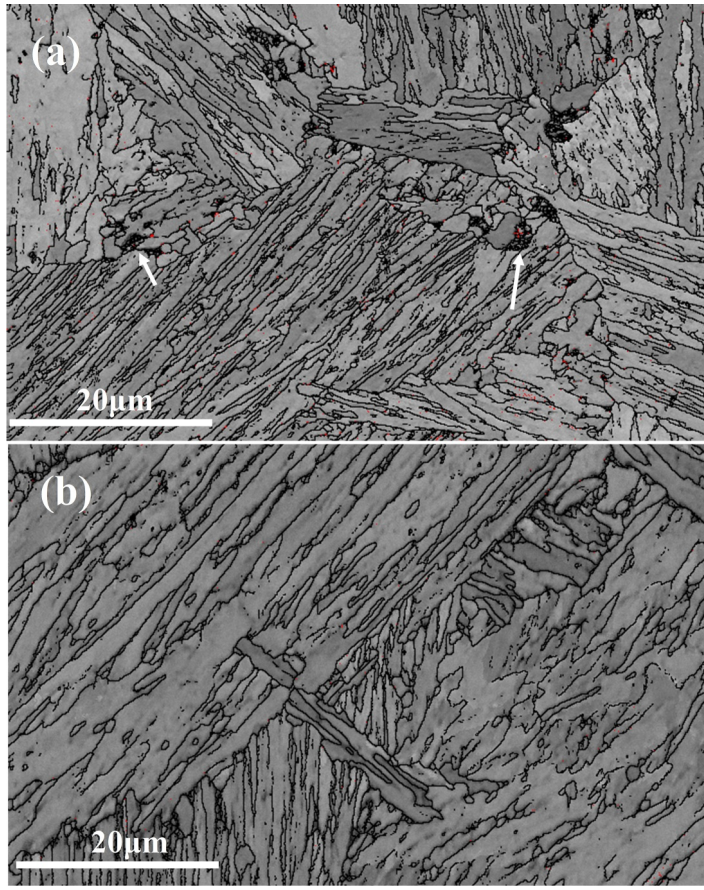

Figure 17. Band contrast maps corresponding to low Ni (a) and high Ni (b) respectively. The dark areas found in massive MA in low Ni indicated by white arrow are confirmed by pole figure analysis to exhibit K-S variants, characteristic of martensite.

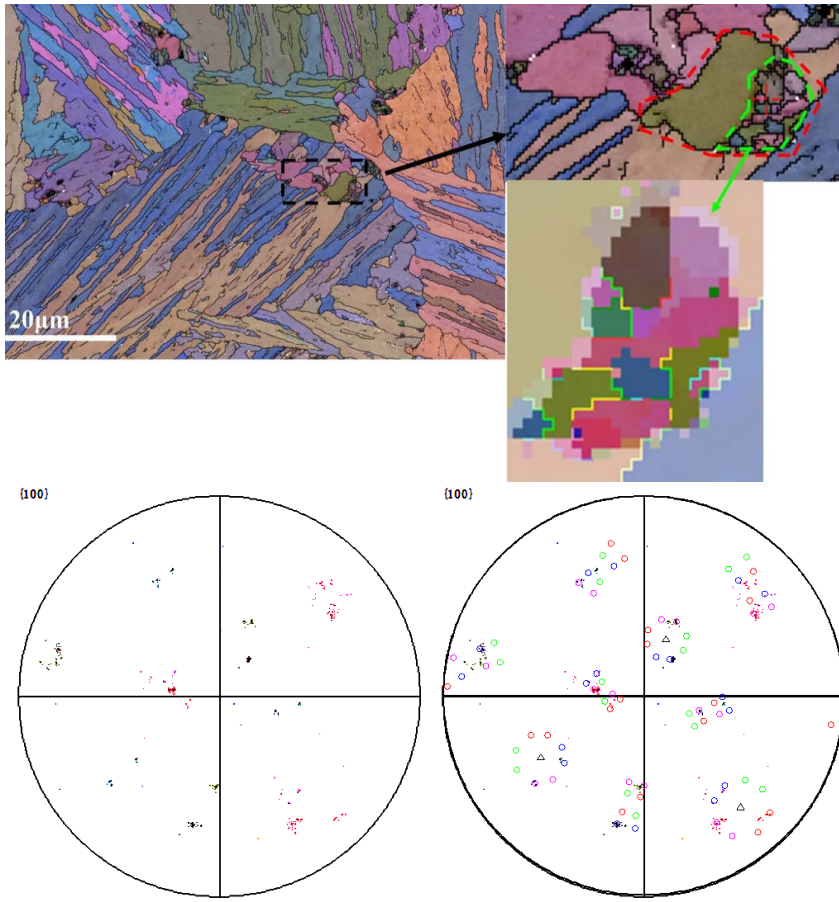

Figure 18. Results of pole figure analysis of dark constituents in Figure 17, which are found to follow K-S variants closely, which is characteristic of martensite.

The chain or necklace–like MA product along austenite grain boundaries is interconnected, providing an easy path for fracture to propagate. The effect of high Ni addition tends to suppress massive MA formation along prior austenite boundaries, while retaining a good amount of high angle boundaries in the matrix. This is identified as the key to improved fracture toughness in inter-critically reheated coarse grained heat affected zone (IRCGHAZ) in multi-pass welding. Aligned MA within the matrix can also give rise to high angle boundaries but these are to be avoided in micro-structural engineering to improve toughness, as high carbon MA is deleterious to toughness.

The low toughness obtained in the IRCGHAZ in low heat input multi-pass girth welding can be suppressed by increasing the Ni content, as demonstrated by the present laboratory Gleeble simulation studies.

Discussion

1. Significance of EBSD Analysis in Structure-Property Correlation Studies in HAZ Simulation

EBSD allows:

(i) Characterization of high angle boundaries super-posed on the microstructure.
(ii) Determination of crystallographic relationships of coherent transformation products with the parent austenite grain.
(iii) Determination of crystallographic misorientations occurring between the packets and within a packet.
(iv) Identification of residual austenite associated with MA product by pole figure analysis.

Since high angle boundaries act as barriers to microcrack propagation, it should be possible, in principle, to control brittle fracture initiation if a microcrack could be arrested by high angle boundaries before it grows to attain the critical Griffith crack length, in accordance with the Cottrell-Petch model of brittle fracture [10]. In the present work, the focus is on retention of toughness in the HAZ by (i) retention of high angle boundaries that act as micro-crack arresters, and (ii) suppression of MA product associated with high carbon martensite, which promotes brittle fracture nucleation.

2. Effect of Niobium on Transformation Temperature

Serin et al. have carried out systematic isothermal and continuous cooling transformation studies in Nb and B containing low carbon (0.1%C, 1.2%Mn) steels and shown that Nb addition to C-Mn steel retards the mean nucleation rate of ferrite per unit boundary area sharply, by a factor of 20, which is comparable to the effect of boron addition [11]. Further, they have shown that interphase precipitation of NbC during transformation retards growth of ferrite by a factor of 4 [12]. Since Nb addition retards the nucleation and growth rate of ferrite, Nb addition to C-Mn steel is very effective in lowering the transformation temperature. The effect of dissolved Nb in retarding austenite to ferrite transformation has since been well established and widely reported [13, 14, 15].

3. Effect of Transformation Temperature on Evolution of Microstructural Morphology and Crystallographic High Angle Boundaries

The results from EBSD analysis of HAZ samples from weld simulation of single pass welding of X100 and X80 HTP plates for a wide range of heat inputs from 8 - 50 kJ/cm are examined in further detail. Figure 19 shows a distinct difference in the distribution of high angle boundaries between the HAZ sample of X100 with an optimum heat input of 20 kJ/cm exhibiting best

toughness compared with other samples of both higher and lower heat input. The fracture surface of the sample with 20 kJ/cm heat input shown in Figure 20 is clearly ductile while samples of lower heat input of 8 kJ/cm and higher heat input of 25 and 50 kJ/cm are clearly brittle. The analysis of the data for austenite grain size (Figure 6b), MA product distribution (Figure 7) and density and dispersion of high angle boundaries (Figure 8) of the four samples has shown that optimum density and dispersion of high angle boundaries is the dominant factor causing the suppression of brittle fracture initiation in the sample with 20 kJ/cm. The HAZ sample with the best toughness exhibits well distributed packets within the austenite grains, each packet exhibiting high angle boundaries between crystallographic units belonging to different Bain groups as identified by different colors in Figure 10, all contributing to a uniform distribution of high density of high angle boundaries.

At higher heat inputs of 25 and 50 kJ/cm, one of the Bain group tends to dominate within the packet, which results in very low density and dispersion of high angle boundaries, see (c) and (d) in Figure 10. The microstructure corresponds to acicular ferrite at higher heat input. At a lower heat input of 8 kJ/cm, one of the Bain group tends to dominate in a packet, and the matrix structure exhibits laths with small misorientations. The microstructure seems to be governed by a displacive mechanism. It should be noted that islands of MA would also form high angle boundaries but hard brittle martensite associated with MA should be avoided as it would nucleate cracks rather than arrest the cracks.

Figure 19 is a composite diagram from Figures 6 and 10, which shows Charpy toughness at -20 ºC as a function of heat input in CGHAZ. The corresponding variation in the distribution of Bain groups within a packet is schematically illustrated for each of the four samples examined with different heat input. The optimum crystallographic structure for maximum toughness is benchmarked corresponding to a cooling rate of 15 ºC/s, which results in an optimum temperature window of transformation. At the lower cooling rate of 2.4 ºC/s corresponding to a very high heat input of 50 kJ/cm, the transformation temperature will be raised, whereupon the mechanism will tend to be one of diffusion control. At higher transformation temperature, non-uniform dispersion and lower density of high angle boundaries occur. At a higher cooling rate of about 60 ºC/s, corresponding to a lower heat input of 8 kJ/cm, the HAZ sample exhibits predominantly one Bain group in a packet and the matrix shows a high density of fine laths with all the laths showing about the same orientation. The transformation will be controlled by a displacive mechanism. By comparison, the sample with 25 kJ/cm exhibits predominantly one Bain group in each packet. The toughness of the sample with the higher heat input of 25 kJ/cm is lower than the sample with a heat input of 8 kJ/cm. This work has shown clearly the differences in the crystallographic structure, which, in turn, are related to the cooling rates associated with different heat inputs, and their effect on toughness properties.

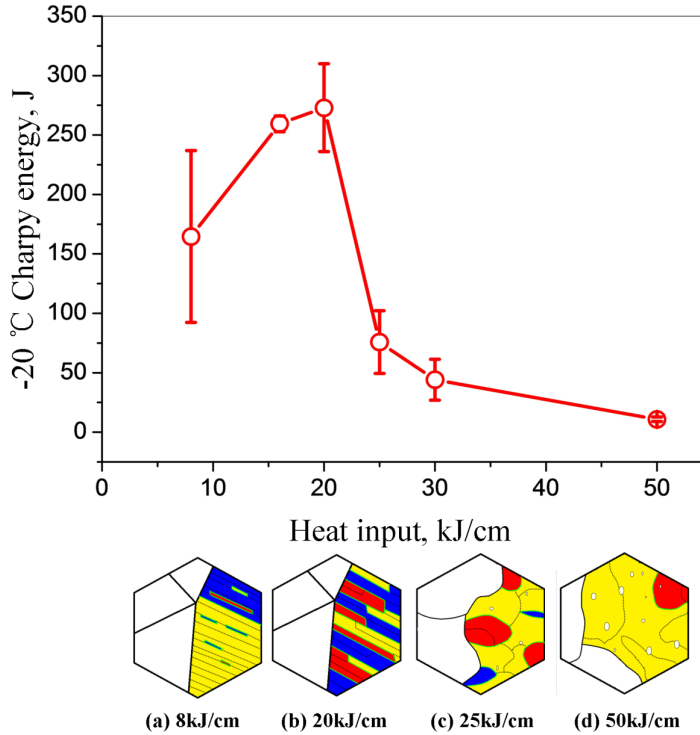

Figure 19. Correlation of crystallographic structure with toughness as a function of heat input in single pass welding.

Figure 20 shows SEM pictures of fracture surfaces of Charpy samples for the four heat inputs. Dimples characteristic of ductile fractures are seen at an optimum heat input of 20 kJ/cm. The transition to brittle fracture can be clearly seen at lower (8 kJ/cm) and higher (25 kJ/cm and above) heat input than 20 kJ/cm.

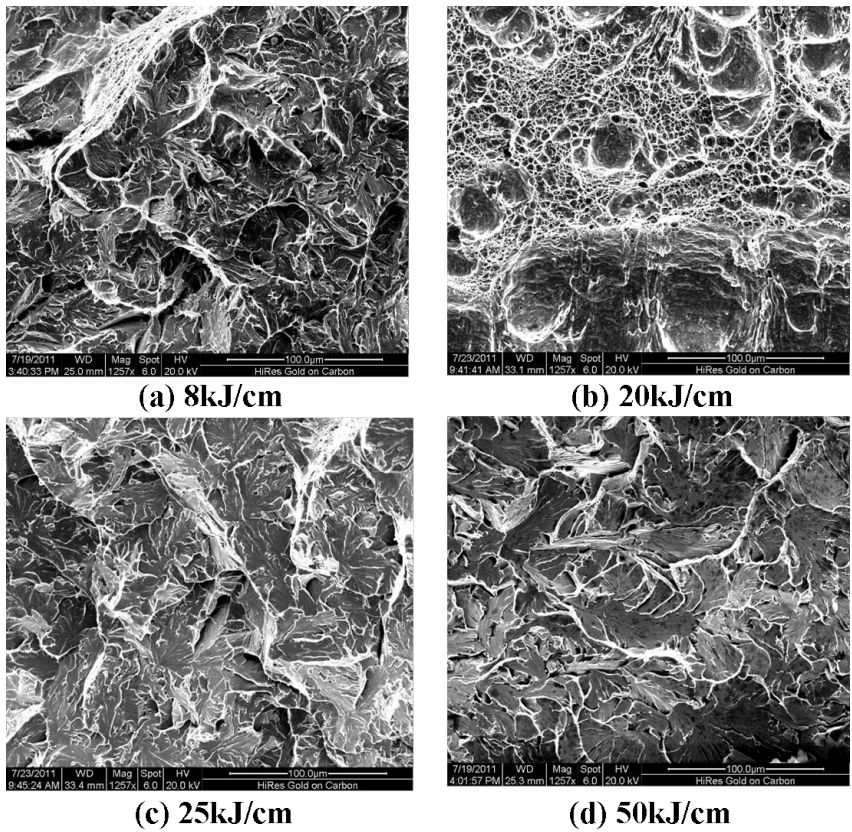

Figure 20. SEM pictures of fracture surfaces from Charpy specimens corresponding to different heat inputs. The maximum toughness is obtained corresponding to ductile fracture at an optimum heat input of 20 kJ /cm.

Figure 21 is a schematic diagram showing the hierarchical evolution of high angle boundaries associated within the microstructure of the HAZ for single-pass welding of HTP, adopting the reference CCT diagram for HTP by Hulka [16]. Higher niobium allows a broad window with a wide range of cooling rates for obtaining the target structure with a good distribution of high angle boundaries caused by different Bain groups within each packet. This turns out to be beneficial in obtaining target crystallographic structures at an optimum heat input of 20 kJ/cm.

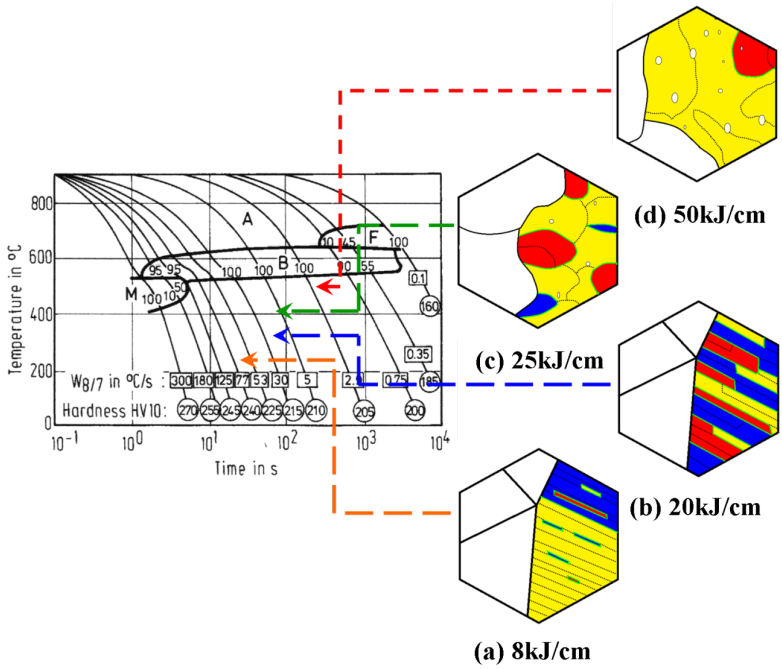

Figure 21. Hierarchical evolution of high angle boundaries associated with the microstructure in the HAZ for single-pass welding of HTP, adopting the CCT diagram of Hulka for HTP [16].

Figure 22 shows schematic diagrams, illustrating the variation in crystallographic distribution of Bain groups corresponding to different mean transformation temperatures, which in turn, is plotted against 50% FATT by Batte and Kirkwood [13]. The target structure for the lowest 50% FATT thus corresponds to the target microstructure with high density and good dispersion of high angle boundaries obtained from an optimum cooling rate, corresponding to the optimum temperature window of transformation.

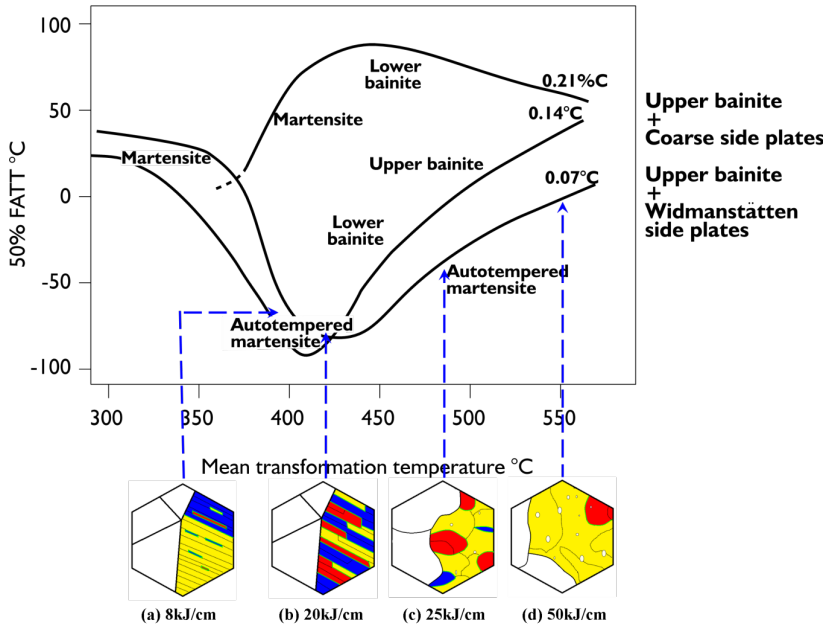

Figure 22. Inter-relationship of temperature of transformation, 50% FATT and microstructure and the crystallographic evolution of high angle boundaries, after Batte and Kirkwood [13].

It is proposed that by lowering the transformation temperature window through the hardenability effect of niobium, coherent transformation with a high density of high angle boundaries, due to large misorientation between different Bain groups, could be promoted.

HTP X80. The same distinguishing features were also found in HAZ samples of HTP X80, between the sample with best toughness at 20 kJ/cm and the sample with the worst toughness at 50 kJ/cm.

The HAZ sample with the worst toughness in HTP exhibited a very low density of high angle boundaries coupled with a high amount of MA. In addition, the austenite grain size is coarse in high heat input welding and the matrix microstructure exhibits granular bainite.

Single Pass Welding of Low Ni Nb Plate. In low heat input (6 kJ/cm) single pass welding of low Ni, Nb microalloyed plate, islands of MA product are identified within a packet, which contributes to the number of high angle boundaries. It should be noted that high angle boundaries associated with MA product should be regarded as “bad” high angle boundary, as MA product enveloped by such a boundary is a crack initiator. Thus only high angle boundaries formed between two blocks, with comparable size and belonging to different Bain groups, are considered to be ideal in the target microstructure.

Low Heat Input Multi-pass Welding of Low Ni Plate. High angle boundaries are formed around aligned MA product within austenite grains and massive MA product is formed at prior austenite grain boundaries. Both are detrimental to fracture toughness. The necklace of massive MA product formed around the prior austenite grains is shown to be suppressed by high Ni addition. In inter-critical reheated coarse grained austenite, high carbon partitioning to residual austenite is predicted, which upon transformation converts to brittle high carbon martensite. Preliminary work has confirmed the presence of martensite by determining the K-S relationship in massive MA. Work is in progress to clarify the mechanism by which Ni suppresses the formation of massive high carbon MA in multi-pass welding under low heat input in Nb microalloyed steels. More research is required to study the effect of the temperature window of transformation on crystallographic high angle boundary evolution, and to get a quantitative understanding of the effect of chemistry and process variables on the evolution of high angle boundaries in HAZ so as to improve HAZ toughness in microalloyed plates.

EBSD studies on laboratory Gleeble samples demonstrate that niobium offers a distinct advantage in lowering transformation temperature in low carbon austenite. This can be used effectively to advantage to promote coherent transformation in austenite to produce a high density and good dispersion of high angle boundaries, which act as micro-crack arresters

Word of Caution in Synthesis

HAZ regions in real welding of linepipes in the mill by moderately high heat input single-pass welding of plates of a wide range of thickness, and in the field by low heat input multi-pass girth welding of pipes, exhibit steep microstructural gradients in narrow zones; therefore caution must be exercised in the application of Gleeble simulation data based on uniform microstructures to field conditions. Microstructural engineering to improve toughness in the HAZ should be based on metallurgical understanding of subtle deviations between the laboratory and field conditions. These require in-depth characterization of microstructure and high angle boundaries associated with them in actual welds.

Conclusions

(1) EBSD studies on HAZ regions of single-pass welding of higher grade linepipe steels of X80 HTP and X100 multi-phase steels based on higher niobium have confirmed that there is an optimum heat input for a given plate thickness at which maximum toughness is obtained corresponding to a high density and dispersion of high angle boundaries, which act as micro-crack arresters, and minimal high carbon MA, which act as brittle fracture initiators.

(2) The target structure for good toughness is characterized by well distributed bainite packets within an austenite grain and more importantly a large number of crystallographic units belonging to different Bain groups occurring within each packet.

(3) High angle boundaries are formed between crystallographic units belonging to different Bain groups within each packet. There is an optimum temperature window of transformation corresponding to an optimum cooling rate in which a large number of crystallographic units belonging to different Bain groups is obtained to give a high density of high angle boundaries.

(4) A high density of high angle boundaries is associated with low temperature transformation product. Niobium addition is beneficial for lowering transformation temperature as niobium dissolved in iron inhibits nucleation of ferrite at austenite grain boundaries and NbC interphase precipitation retards growth of ferrite. Thus the target structure with a high density and dispersion of high angle boundaries can be promoted with ease in higher grade linepipe steels microalloyed with higher niobium.

(5) In multi-pass low heat input inter-critically reheated coarse grained heat affected zone IRCGHAZ, the loss of toughness is caused by a high volume fraction of high carbon MA, associated with massive MA at austenite grain boundaries and aligned MA product in the matrix. Nickel addition is shown to be beneficial in suppressing high carbon massive MA, which occurs as a necklace of precipitates along the austenite boundary.

(6) It is demonstrated that pole figure analysis can be used judiciously to discriminate "good" high angle boundaries associated with different Bain groups that act as micro-crack arresters from "bad" high angle boundaries associated with high carbon MA products that could initiate cracks.

Acknowledgements

The authors wish to acknowledge with grateful thanks the funding and technical support from (i) CBMM, Brazil, (ii) Chinese Government scholarship, (iii) Evraz Inc NA, Regina, (iv) Sha Steel Company, Jiangsu, China and (iv) NSERC, Canada. Special thanks are due to Chris Butcher, Glynis de Silveira and G. Botton of CCEM, Brockhouse Institute for Materials Research, McMaster University, Canada for electron optics support.

References

1. F. Hamad, L. Collins and R. Volkers, "Effects of Gas Metal Arc Welding Procedure on the Heat-Affected Zone (HAZ)," *Proceedings of International Pipeline Conference 2008*, Calgary, Alberta, Canada, (2008), 1-17.

2. F. Fazeli et al., "Modeling the Effect of Nb on Austenite Decomposition in Advanced Steels," *Proceedings of AIST International Symposium on the Recent Developments in Plate Steels 2011*, Winter Park , Colorado, USA, (19-22 June 2011), 343-350.

3. C. Penniston, L. Collins and F. Hamad, "Effects of Ti, C and N on Weld HAZ Toughness of High Strength Line," *Proceedings of International Pipeline Conference 2008*, Calgary, Alberta, Canada, (2008), 1-9.

4. C. Penniston and L.E. Collins, "Field Girth Weld HAZ Toughness Improvement – X80/Grade 550," *Proceedings of International Pipeline Conference 2010*, Calgary, Alberta, Canada, (2010), 1-9.

5. Z. Guo, C.S. Lee and J.W. Morris Jr., "On Coherent Transformations in Steel," *Acta Materialia*, 52 (2004), 5511-5518.

6. A.F. Gourgues, H.M. Flower and T. C. Lindley, “Electron Backscattering Diffraction Study of Acicular Ferrite, Bainite and Martensitic Steel,” *Materials, Science and Technology*, 16 (2000), 26-40.

7. H. Kitahara et al., “Crystallographic Features of Lath Martensite in Low-Carbon Steel,” *Acta Materialia*, 54 (2006), 1279-1288.

8. V. Pancholi et al., “Self-Accommodation in the Bainitic Microstructure of Ultra-High-Strength Steel,” *Acta Materialia*, 56 (2008), 2037-2050.

9. Y. Li et al., “The Effect of Vanadium and Niobium on the Properties and Microstructure of the Intercritically Reheated Coarse Grained Heat Affected Zone in Low Carbon Microalloyed Steels,” *The Iron and Steel Institute of Japan International*, 41 (1) (2001), 46-55.

10. A. Cottrell, “Brittle Fracture from Pile-ups in Polycrystalline Iron,” Chapter 7 in Book on *Yield, Flow and Fracture of Polycrystals*, ed. T.N. Baker (Applied Science Publishers, 1983), 123-129.

11. B. Serin et al., “The Transformation Characteristics and Properties of Low Carbon Steels containing niobium and boron,” *Memoires Scientifiques de Le Revue de Metallurgie*, 75 (June 1978), 355-369.

12. R.W.K. Honeycombe, “Transformation from Austenite in Alloy Steels,” *Metallurgical Trans*actions, 7A (1976), 915-936.

13. A.D. Batte and P.R. Kirkwood, “Developments in the Weldability and Toughness of Steels for Offshore Structures,” *Proceedings of Microalloying ‘88 held in conjunction with the 1988 World Materials Congress*, Chicago, Illinois, USA, (September 1988).

14. W.J. Poole et al., “Microstructure Evolution in the HAZ of Girth Welds in Linepipe Steels for the Arctic,” *Proceedings of 8th International Pipeline Conference 2010*, Calgary Alberta, Canada, (2010).

15. Y.Q. Zhang et al., “Effect of Heat Input on Microstructure and Toughness of Coarse Grain Heat Affected Zone in Nb Microalloyed HSLA Steels,” *Journal of Iron and Steel Research International*, 16 (5) (2009), 73-80.

16. K. Hulka, “The Role of Niobium in Low Carbon Bainitic HSLA Steel,” *Proceedings of 1st International Conference on Super-High Strength Steels 2005*, Rome, Italy, (November 2005).